22.4 A WiFi and Bluetooth Backscattering Combo Chip Featuring Beam Steering via a Fully-Reflective Phased-Controlled Multi-Antenna Termination Technique Enabling Operation Over 56 Meters

Shih-Kai Kuo*, Manideep Dunna*, Dinesh Bharadia, Patrick P. Mercier

University of California, San Diego, CA

*Equally-Credited Authors (ECAs)

Many envisioned IoT applications are not realizable today due to the mW-level power burden of wireless communication circuits for the most popular consumer standards: WiFi and BLE. To help enable new IoT applications, WiFi backscatter communication techniques have been shown to enable a ~1,000× reduction in power consumption over conventional transceivers while maintaining WiFi standard compatibility [1-3]. However, pragmatic deployment is currently hindered by their limited range, and lack of IC implementations for BLE [4-5]. For example, [3] and [1] only operate with inter-access point (AP) distances of 16m and 21m, respectively, which is not quite sufficient for robust operation in dense office environments, or large smart warehouses or airports with larger (and therefore lower cost) inter-AP deployment distances. Since backscatter modulation is passive with no RF power amplification, additional range can only be achieved by reducing insertion loss or adding antenna gain. For example, the work in [2] replaced 50Ω absorbing terminations with reactive terminations to reduce insertion loss over [1] and improve range to 26m, though a bulky and lossy Wilkinson power splitter/combiner was still required. The work in [2] also introduced a way to utilize multiple antennas to achieve MIMO-like antenna gain, though only in a static retro-reflective manner with no beam steering capabilities. This latter approach requires two co-located APs, which have self-interference challenges, and are thus not readily available in existing mesh networks. In addition to range challenges, there are no current backscatter ICs that can operate with BLE.

This paper introduces a single backscatter IC that: 1) unlocks the maximum possible range for single-antenna single-side-band (SSB) QPSK backscatter solutions via a transmission-line-less {0,90,180,270}° multiplexed reactive termination approach with 3dB improved insertion loss over the approach in [2]; 2) enables beamscattering: dynamically-controllable beam steering for multi-antenna SSB QPSK Wi-Fi backscatter solutions via an array of four multiplexed reactive termination networks driven by a phased IF I/Q generator; and 3) includes a BLE-compatible wakeup RX and FSK backscatter modulation for compatibility with BLE devices. The system design contribution is presented in [6].

Figure 22.4.1 (left) shows the absorbing termination approach of [1] in contrast to the proposed single-antenna approach (Fig. 22.4.1 middle-right). In [1], the incident signal (e.g., WiFi Ch. 6) is divided into I and Q paths at RF via a power splitter. The top I path is terminated by either a 50Ω resistor (reflection coefficient $\Gamma = 0$) or a 1.2pF capacitor at 2.4GHz ($\Gamma = e^{j\times-90°}$ at 2.4GHz), while the bottom Q path is terminated by either a 50Ω resistor ($\Gamma = 0$) or an open circuit ($\Gamma = e^{j\times0°}$), depending on the IF clock and the tag data. Power splitting and absorbing terminations by definition reduce reflected signal power, leading to a larger effective insertion loss. While the absorbing termination in [1] was replaced by fully reflecting loads in [2], a lossy power splitter was still utilized to create I/Q paths. In this work, the power splitter is eliminated through the realization that I/Q combination does not have to occur at RF, but can instead occur at baseband. Thus, a single SP4T switch, if driven with the correct timing, can cycle through open ($\Gamma = e^{j\times0°}$), short ($\Gamma = e^{j\times180°}$), capacitive ($\Gamma = e^{j\times-90°}$), or inductive ($\Gamma = e^{j\times+90°}$) terminations to generate the same SSB QPSK modulation as [2], but now with 3dB lower insertion loss.

In applications where there is room for multiple antennas, [2] demonstrated that MIMO antenna gain is possible through a retro-reflective IQ-modulated Van Atta array utilizing fixed-delay transmission lines connected to alternate antennas for SSB QPSK modulation (Fig. 22.4.1 middle-left). However, fixed-delay transmission lines occupy a large board area and, more importantly, are not tunable. As a result, beam steering is not possible, and co-located APs (which have difficult self-interference challenges in current commodity hardware) are required.

This work presents a design that enables beam steering, along with the corresponding MIMO antenna gain, to enable long-range deployment regardless of specific AP location/orientation in a passive WiFi backscatter system. The proposed beamscattering concept (Fig. 22.4.1, right) leverages multiple copies of the proposed fully-reflective SP4T termination, where the relative timing of the switches are carefully set by a phase controller. By delaying the timing of reflections by a controllable phase (Δ), in-air power can be added constructively in specific, controllable directions, as illustrated in Fig. 22.4.2. When the antennae are separated by distance L, the steering direction can be determined with the formula shown in Fig. 22.4.2 (top left). For example, when $\Delta=30°$, the beam can be steered by 10° when L= λ/2 at 2.4GHz.

To enable beamscattered SSB modulation to an adjacent WiFi channel (e.g., a 25MHz frequency translation from Ch. 6 to Ch. 11) without requiring an explicit external tone generator as in [3], all while having a controllable Δ with a resolution of 15°, a set of 50MHz clocks with 30° phase differences {0,30,60,90,120,150}° is tapped out from a 6-stage differential ring VCO in a type-II PLL, as shown in Fig. 22.4.2 (bottom left). Each clock from the set is further fed into a divide-by-2 block, which produces quadrature 25MHz clocks, such that 15° phase resolution is available. As shown in Fig. 22.4.2 (bottom right), angle selection bits (5-1 muxes) and plus-minus control bit (4-1 muxes) that control leading/lagging conditions at each reflector allow 10 possible permutations of Δ from -75° to +75°. The Q portion is replicated with a 90° shift from the I portion to implement QPSK SSB backscatter. Note that the open reflection condition ($\Gamma = e^{j\times0°}$) does not require an explicit switch, as all 3 switches can be opened to achieve this state.

In applications where WiFi signals are not readily available (e.g., with wearable devices), emerging applications desire the ability to communicate via BLE. However, unlike WiFi, which uses phase-based modulation, BLE utilizes FSK with 0.5MHz tone separations (Fig. 22.4.3 bottom left), and thus a different backscatter modulation technique is required. In this work, the incident signal (e.g., at BLE Ch. 37) is SSB-frequency-translated to another channel $f_{IF,OUT}$ away (e.g., Ch. 38) with the following codeword translation scheme: when the tag data is 0, the incident signal is left undisturbed, and when the tag data is 1, the incident FSK tone frequency should be translated to the opposite FSK tone frequency (Fig. 22.4.3 bottom). However, since the incident data is unknown to the tag, an XOR gate is used to mix 0.5MHz with $f_{IF,OUT}$ so that no matter what the incident bit is, the backscatter bit can always be generated, with an image lying outside the receiver channel when the tag data is 1 (which can be filtered by the BLE RX).

The proposed WiFi/BLE backscattering combo chip, whose block diagram is shown in Fig. 22.4.3 (top left), is woken up by a pre-specified sequence of WiFi or BLE packets by using an ED-first architecture with a counter-based correlator that is immune to the uncertainty of packet gap lengths. After the tag is woken up, it can be either used in WiFi or BLE mode, with the beam steering option available in WiFi mode. There are two implementation of the BLE modulator included: 1) a BLE-only mode, where it is more hardware efficient to implement as a one-bit multiplexer that select either $f_{IF,OUT}$ or $f_{IF,OUT}$ ±0.5MHz based on the tag data; or 2) when QPSK WiFi is also needed in a combo-chip, it is more hardware efficient to reuse the QPSK WiFi modulator by applying the XOR function with one input using the BLE tag data, and the other set to 0.

The proposed backscatter IC was fabricated in 65nm, occupying 0.42 mm². Figure 22.4.4 (top left) shows how incident 802.11b WiFi signals at Ch. 6 can be translated to either Ch. 1 or Ch. 11 (residual power at Ch. 6 due to close distance between TX and RX during indoor wireless testing) with >14dB sideband rejection, all while enabling beam steering with >10dB improved output power compared to a single-antenna solution. The resulting beam pattern for various Δ configurations are shown in Fig. 22.4.4 (bottom) and compared to theoretical results, showing excellent agreement. Figure 22.4.4 (top right) also shows representative BLE packet translations from Ch. 38 to Ch. 37.

Wireless system-level measurements in Fig. 22.4.5 with COTS AP hardware show a representative example of successful packets received for a 23m TX-to-tag and 35m tag-to-RX setup, resulting in a worst case AP-to-AP distance of 56m (when the tag is in the middle between equidistant APs). Figure 22.4.5 (right) shows the maximum wireless tag-to-RX range achieved by the beam steering tag in different directions for four different steering angles (+25°,+5°,-5°,-25°) in comparison with a single antenna tag which achieves a 35m AP-to-AP distance regardless of orientation. Figure 22.4.5 also shows successful wirelessly decoded BLE packets at a BER of 2x10⁻⁴. The IC consumes 39µW and 88µW for single- and multi-antenna approaches, respectively, which is still ~1,000× lower power than conventional WiFi TXs, and ~100x lower power than conventional BLE TXs. Figure 22.4.6 compares results to prior work, showing the longest achieved range of prior-art WiFi backscatter chips, and the first WiFi/BLE combo operation. A die micrograph is shown in Fig. 22.4.7.

References:
[1] P.-H. Wang et al., "A 28µW IoT Tag that can Communicate with Commodity WiFi Transceivers via a Single-Side-Band QPSK Backscatter Communication Technique," *ISSCC,* pp. 312-314, Feb. 2020.
[2] M. Meng et al., "Improving the Range of WiFi Backscatter Via a Passive Retro-Reflective Single-Side-Band-Modulating MIMO Array and Non-Absorbing Termination," *ISSCC,* pp. 202-204, Feb. 2021.
[3] L. Lin et al., "Battery-Less IoT Sensor Node with PLL-Less WiFi Backscattering Communications in a 2.5-µW Peak Power Envelope," *VLSI Symp.,* 2021.
[4] M. Zhang et al, "Reliable Backscatter with Commodity BLE," IEEE INFOCOM 2020.
[5] M. Zhang et al., "Commodity-level BLE backscatter," ACM Mobisys 2021.
[6] M. Dunna et al., "BeamScatter: Scalable, Deployable, Long-Range Backscatter Communication with Beam Steering", Arxiv:2110.14585v1, Oct. 27, 2021.
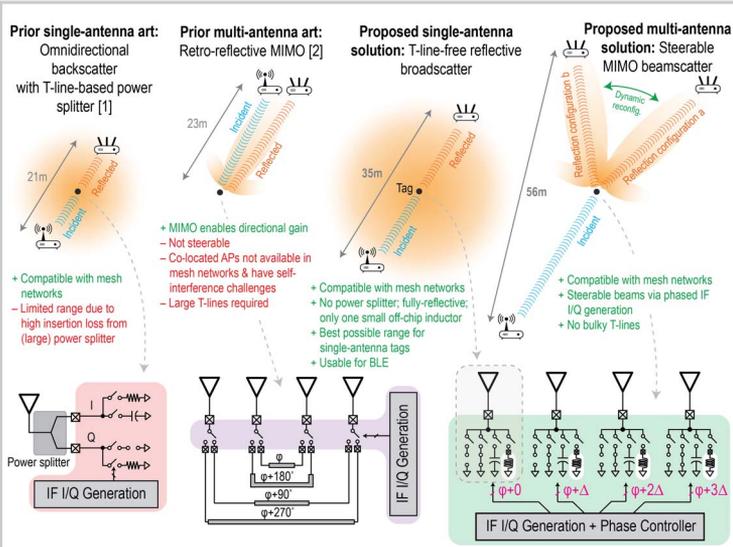
Figure 22.4.1: Prior-art omnidirectional and retro-reflective MIMO backscatter approaches (left); proposed transmission-line-free fully reflective broadside scattering and steerable MIMO directional beam scattering approaches (right).
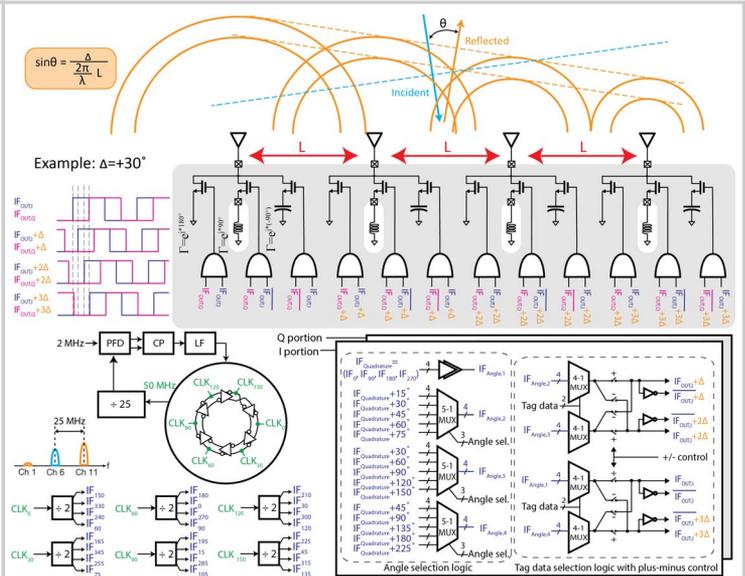

Figure 22.4.2: Schematic of the frequency and phase shifting beamscatter circuit enabling configurable beam steering for WiFi backscatter.
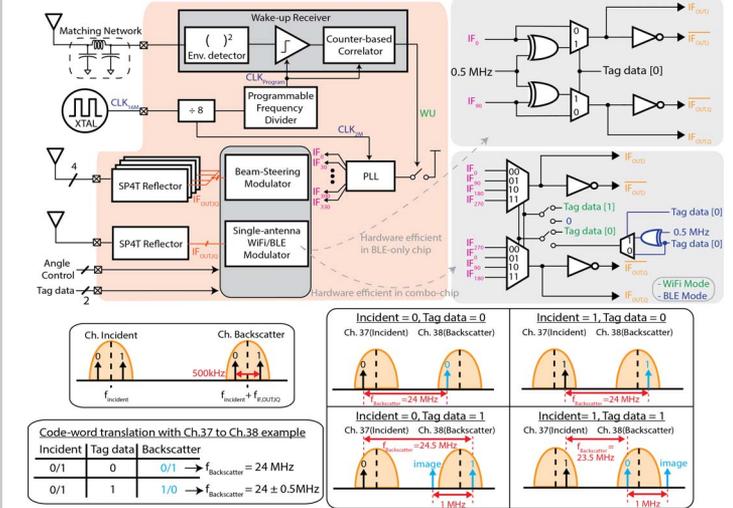

Figure 22.4.3: Overall system block diagram including a WiFi/BLE wake-up receiver, an on-chip multi-phase PLL, a multi-antenna WiFi beam steering block, and a single-antenna WiFi/BLE combo modulator (top); modulation and codeword translation scheme for BLE backscatter (bottom).
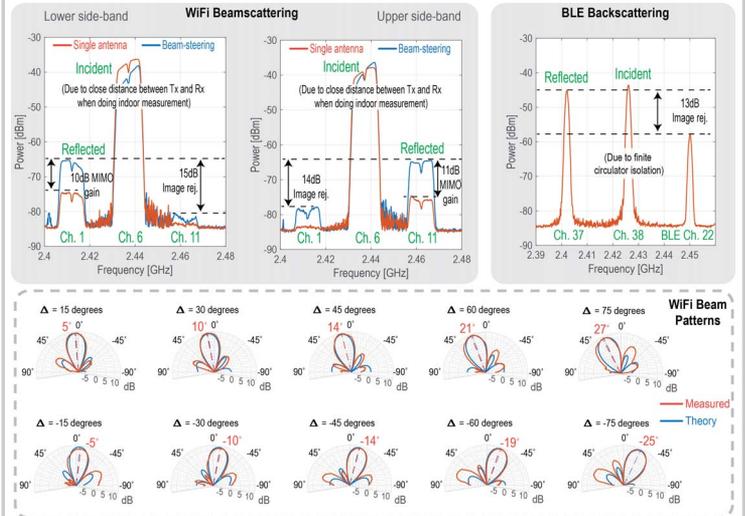

Figure 22.4.4: Measured SSB wireless spectra for beamscattered and broadscattered WiFi (top left) and broadscattered SSB BLE (top right); measured WiFi beamscattered patterns compared to theoretical results (bottom).
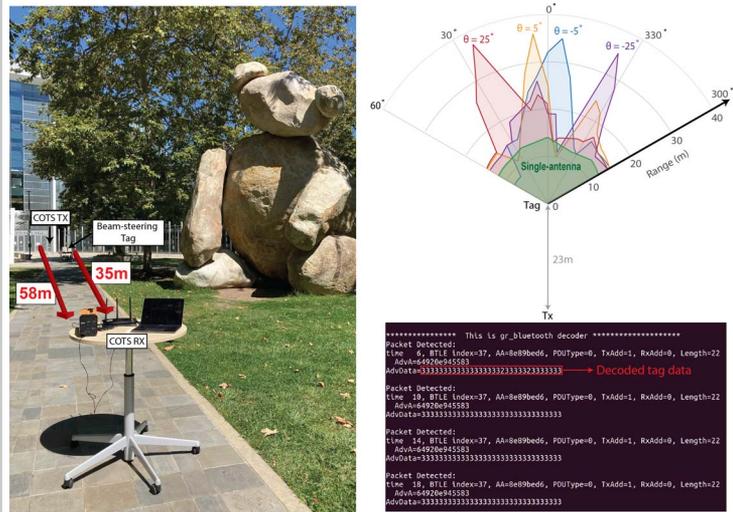
22

Figure 22.4.5: Wireless experiment demonstrating successful 23m TX-to-tag and 35m tag-to-RX operation (left); maximum operation distance chart for various beam steering angles (top right); demonstration of successfully decoded BLE packets (BER=2e-4) frequency translated from Ch. 38 to Ch. 37 (bottom right).

Figure 22.4.6: Table of comparisons to prior-art standards-compatible backscatter ICs.

	[1]	[2]		[3]	This Work	
Technology	65 nm	65 nm		180 nm	65 nm	
Core Area (mm²)	0.34	0.41		1.62	0.42	
Backscatter Scheme	Partially Absorbing QPSK	Fully Reflective QPSK	Retro-reflective MIMO QPSK	DBPSK	QPSK Fully-reflective MIMO Beam-steering for WiFi	
					SSB FSK for BLE	
Single Side Band?	Yes	Yes	Yes	No	Yes	
Max Data Rate	2 Mbps	2 Mbps		1 Mbps	WiFi	2 Mbps
					BLE	500 Kbps
Incident Source	WiFi	WiFi		Tone Generator	WiFi or BLE	
AP-to-AP Range with tag in the middle (m)	21	26 (Single-antenna)	23 (MIMO Co-located AP)	16	Single antenna	35
					Beam-steering	56
BLE Compatibility	N/A	N/A		N/A	Yes	
WiFi Compatibility	Yes	Yes	Yes	Yes	Yes	
Compatible with commodity hardware	Yes	Yes	Partial*	No - tone generator needed	Yes	
Wake-up Power (µW)	2.8	4.5		0.15	5.5	
Backscatter Communication Power (µW)	28	32	38	2.5	WiFi/BLE w/ single antenna	39
					WiFi Beam-steering	88

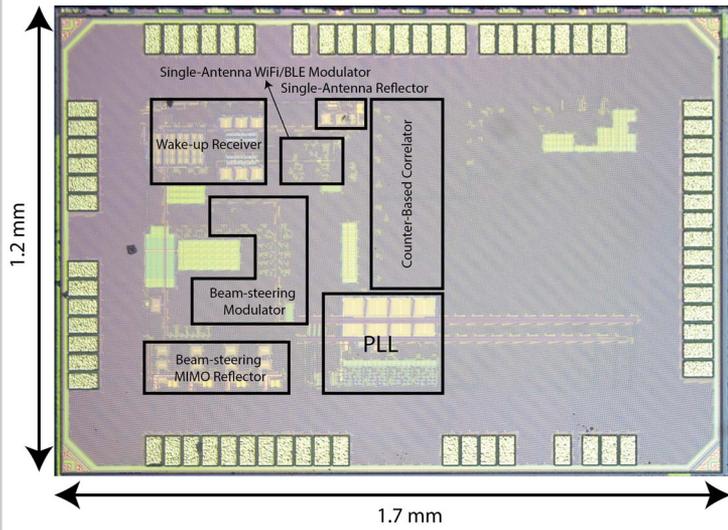* Two co-located commodity APs required with additional shielding between them

Figure 22.4.7: Die micrograh of the WiFi/BLE backscattering combo chip.